INTERNATIONAL JOURNAL OF PRECISION ENGINEERING AND MANUFACTURING Vol. 17, No. 8, pp. 1017-1024 AUGUST 2016 / 1017
DOI: 10.1007/s12541-016-0124-7 ISSN 2234-7593 (Print) / ISSN 2005-4602 (Online)

Performance Improvement of an Oil Pump: Design of Port Assembled with Gerotor (2-Ellipses-Combined Lobe)

Hyo-Seo Kwak[1], Sheng-Huan Li[1], and Chul Kim[2,#]

1 Department of Mechanical Convergence Technology, Pusan National University, 2, Busandaehak-ro 63beon-gil, Geumjeong-gu, Busan, 46241, South Korea
2 Research Institute of Mechanical Technology, Pusan National University, 2, Busandaehak-ro 63beon-gil, Geumjeong-gu, Busan, 46241, South Korea
Corresponding Author. E-mail: chulki@pusan.ac.kr, TEL: +82-51-510-2489, FAX: +82-51-512-9835

KEYWORDS: Oil pump, Port, Gerotor, CFD analysis, Flow rate, Irregularity

An internal gerotor pump is used to enhance the oil hydraulics of machine tools, automotive engines and compressor. In particular, this type of pump is used to supply lubricants in an automotive engine. Recently, improvements in automobile fuel efficiency and the reduction of noise have become critical issues. Thus, gerotor internal oil pumps have been studied for high flow rate and low noise through designs of multiple combined lobe shapes. In this study, in order to address the problems of existing oil pumps, design of a new lobe shape with 2-ellipses was developed in order to decrease a sharp change of curvature. Performance parameters of an improved gerotor (2-ellipses) were calculated and compared with those of the existing gerotor (circle and 3-ellipses). Also, we performed a computational fluid dynamics (CFD) analysis of an oil pump with the improved gerotor 2-ellipses-combined lobe shape. By using the commercial software ANSYS CFD, geometric parameters relating to the port shape, which affect the performance of flow rate and irregularity, were investigated. A re-design of the port shape was performed in order to improve fuel efficiency and reduce the noise of the oil pump.

Manuscript received: December 3, 2015 / Revised: March 25, 2016 / Accepted: April 4, 2016

1. Introduction

An internal gerotor pump is suitable for enhancing the oil hydraulics of machine tools, automotive engines, compressors, and various other applications. In particular, a pump is an essential machine for supplying lubricants in an automotive engine.[1] In the automobile industry, increased fuel efficiency and the reduction of noise, have become critical issues, so gerotor internal oil pumps have been studied using the optimal design of multiple combined lobe shapes. In previous studies of gerotors,[2-5] new automated design and multiple calculation programs using rotation and translation algorithms have been developed, and two types of combined lobe shapes (ellipse1-involute-ellipse2 and 3-ellipses types) have been generated. The existing 3-combined lobe shapes have a negative effect on performance parameters due to the drastic change of curvature at the point where different profiles combine.[6] Also, in previous studies of the port shapes of oil pumps, fluid analyses have been performed in order to understand flow characteristics (flow rate, pressure pulsation, and velocity) according to rotation angles of the rotor, the temperature of the working oil, and the tip clearance.[7-12] However, a design of a port shape for improving fuel efficiency and reducing noise has not yet been reported in the literature.

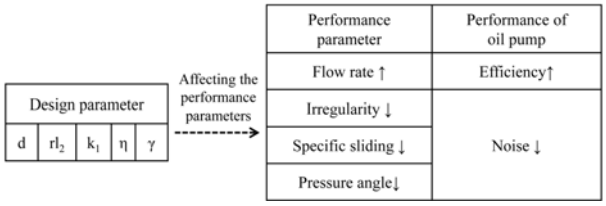

Fig. 1 The causes and effects regarding to the design parameters and performances of oil pump

In this study, to address these problems with existing oil pumps, a design of a new lobe shape with 2-ellipses was developed in order to decrease the sharp change of curvature. Performance parameters of an improved gerotor (2-ellipses) were calculated and compared with those of an existing gerotor (circle and 3-ellipses). The design parameters ("d, "rl_2, "k_1", "γ" and "η") affect the performance parameters (flow rate, irregularity, specific sliding and pressure angle), which influence on efficiency and noise in oil pump. The causes and effects regarding to the design parameters and performances are summarized as Fig. 1.

Also, four geometric parameters relating to the port shape of the oil pump, assembled with the improved gerotor with 2-ellipses combined

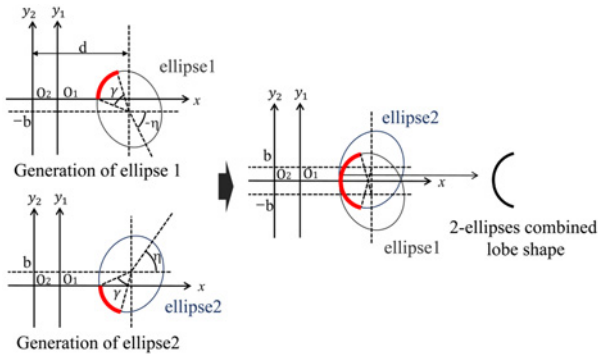

Fig. 2 Generation of a 2-ellipses-combined lobe shape

lobe shape, were suggested for improving performance parameters. The effect of these parameters on flow rate and irregularity were investigated by performing computational fluid dynamics (CFD) analysis using the commercial software ANSYS CFD (14.5ver, ANSYS, Inc., Canonsburg, PA, USA). In order to maximize the reduction of noise, the oil pump was proposed, considering all the geometric parameters which enable irregularity to be decreased.

2. Design of 2-Ellipses-Combined Lobe Shape

2.1 Shape functions of 2-ellipses-combined lobe shape[13]

The lobe shape of the outer rotor is combined with 2-ellipses using a rotation and translation algorithm. The shape is composed of ellipse 1 and ellipse 2, as shown in Fig. 2. In order to derive the shape of ellipse 1, the ellipse rotated η degrees in a clockwise direction on its own center, and moved -b in the y-direction. Ellipse 2 and ellipse 1 are symmetric with respect to the x-axis. The lobe shape of the outer rotor, combined with ellipse 1 and ellipse 2, is obtained. γ is an insertion angle of the ellipse, d is a distance between the center of the outer rotor and curvature center of the outer rotor lobe (ellipse), rl_2 is a radius of the outer rotor lobe, and k is a ellipse's major-to-minor axis ratio.

2.2 Constitutive equations for contact point of 2-ellipses

Theory of Camus is that the direction vector from a point on an outer lobe shape to the pitch point ($\overrightarrow{V_1}$) should be perpendicular to the vector at the point on the ellipse ($\overrightarrow{V_2}$). The case of a circular lobe shape is satisfied with theory of Camus as shown in Fig. 3(a). But, in the case of a 2-ellipses combined lobe shape, the normal line at a contact point is not directed toward the center of the ellipse, as shown in Fig. 3(b). Therefore, the lobe shape rotates θ degree, which $\overrightarrow{V_1}$ should be perpendicular to $\overrightarrow{V_2}$ in order to satisfy theory of Camus within the range, 10^{-6}, using the Newton-Raphson method. In the case of not being satisfied with the range, an inner rotor is generated as shown in Fig. 4. α is an angle between P_2 and the center point (O_2) of the outer rotor. The coordinates (C_{e1}, C_{e2}) of each contact point of ellipse 1 and 2 are then calculated.

2.3 Generation of inner rotor and outer rotor profiles

Using Eqs. (1)~(5), the profile of the inner rotor is generated by rotating α' clockwise from the contact point, (C_{e1}, C_{e2}), on the center

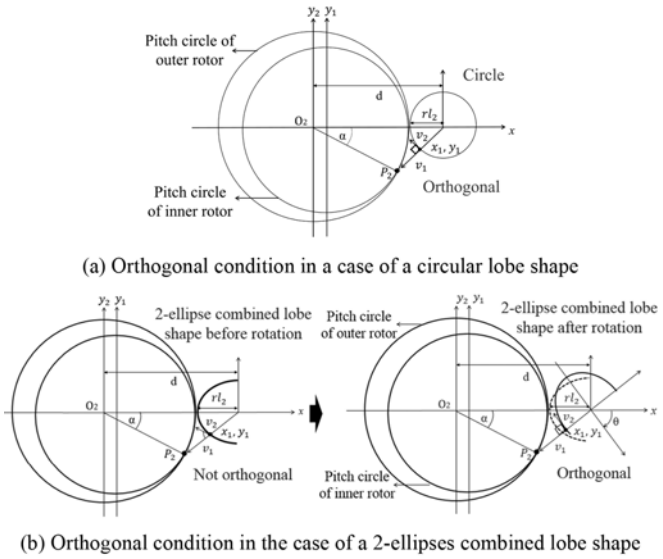

Fig. 3 Orthogonal condition for finding contact points

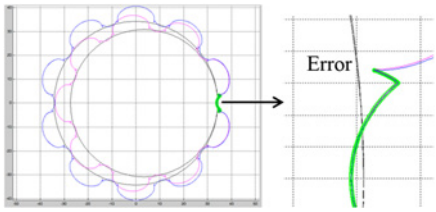

Fig. 4 Error of gerotor shape not satisfied with theory of Camus

(O_1) of the inner rotor. The profile of the outer rotor is generated by rotating α clockwise from the contact point on the center of outer rotor, as shown in Fig. 5. r_1 and r_2 are the radii of the pitch circle of the inner and outer rotor, respectively, and e is the amount of eccentricity.

$$\alpha' = \alpha\left(1-\frac{r_2}{r_1}\right) \tag{1}$$

$$\begin{pmatrix} x_{in} \\ y_{in} \end{pmatrix} = \begin{pmatrix} \cos\alpha' & -\sin\alpha' \\ \sin\alpha' & \cos\alpha' \end{pmatrix} \begin{pmatrix} x_{c,e1,e2}-e \\ y_{c,e1,e2} \end{pmatrix} + \begin{pmatrix} e \\ 0 \end{pmatrix} \tag{2}$$

$$\begin{pmatrix} x_{out} \\ y_{out} \end{pmatrix} = \begin{pmatrix} \cos\alpha & -\sin\alpha \\ \sin\alpha & \cos\alpha \end{pmatrix} \begin{pmatrix} x_{c,e1,e2} \\ y_{c,e1,e2} \end{pmatrix} \tag{3}$$

where

$$\begin{aligned} x_{c,e1} = {} & [(d-rl_2\cdot\cos\theta')\cdot\cos\eta - k\cdot rl_2\cdot\sin\theta' \\ & \cdot\sin\eta]\cdot\cos\alpha - [(d-rl_2\cdot\cos\theta')\cdot\sin\eta \\ & + k\cdot rl_2\cdot\sin\theta'\cdot\cos\eta - b]\cdot\sin\alpha \end{aligned} \tag{4}$$

$$\begin{aligned} y_{c,e1} = {} & [(d-rl_2\cdot\cos\theta')\cdot\cos\eta - k\cdot rl_2\cdot\sin\theta' \\ & \cdot\sin\eta]\cdot\sin\alpha - [(d-rl_2\cdot\cos\theta')\cdot\sin\eta \\ & + k\cdot rl_2\cdot\sin\theta'\cdot\cos\eta - b]\cdot\cos\alpha \end{aligned} \tag{5}$$

$$\begin{aligned} x_{c,e2} = {} & [(d-rl_2\cdot\cos\theta')\cdot\cos\eta + k\cdot rl_2\cdot\sin\theta' \\ & \cdot\sin\eta]\cdot\cos\alpha - [-(d-rl_2\cdot\cos\theta')\cdot\sin\eta \\ & + k\cdot rl_2\cdot\sin\theta'\cdot\cos\eta + b]\cdot\sin\alpha \end{aligned}$$

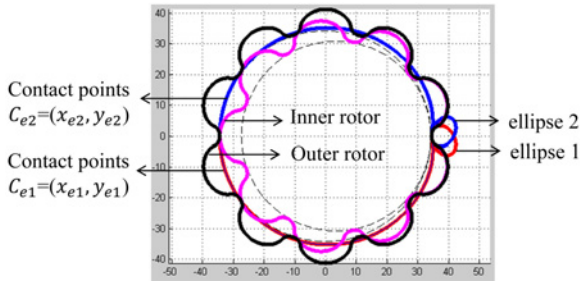

Fig. 5 Inner rotor and outer rotor profiles (2-ellipses)

$$y_{c,e2} = [(d - rl_2 \cdot \cos\theta') \cdot \cos\eta + k \cdot rl_2 \cdot \sin\theta' \cdot \sin\eta] \cdot \sin\alpha - [-(d - rl_2 \cdot \cos\theta') \cdot \sin\eta + k \cdot rl_2 \cdot \sin\theta' \cdot \cos\eta + b] \cdot \cos\alpha$$

3. Design of Gerotor having 2-Ellipses-Combined Lobe Shape

3.1 Performance

The hatched area (q) in Fig. 6, which is between the inner rotor and outer rotor, is increased and decreased according to the rotation of the rotor. The suction and exhaust area is in proportion to the distances between the centers of the inner and outer rotors (O_1 and O_2) and contact points (M and N). Thus, the flow rate (Q) and irregularity (i) are calculated by using Eqs. (6) and (7) where b and ω_1 are the thickness and rotation velocity of the gerotor, respectively, and Z_1 is the tooth number of the inner rotor and Z_2 is that of the outer rotor. Specific sliding represents the ratio of the movement distance of the outer rotor (S_2) and the inner rotor (S_1), according to the rotation of rotor, as shown in Fig. 7[13] and is calculated by Eq. (8). The pressure angle (δ), shown in Fig. 8, is the angle between the line connecting the center of the rotor to the point of intersection (rotor profile and pitch circle) and the line tangent to the point of intersection, and is calculated by using Eqs. (9)~(11) as follows:

3.2 Improved design of gerotor with 2-ellipses-combined lobe shape

Performances of the improved gerotor with 2-ellipses-combined lobe shape, which were developed through the automated design and multiple calculation program, are illustrated in Fig. 9 and Table 1. These performances were compared to those of an existing gerotor with a circle lobe shape. Although the irregularity of 2-ellipses increases by 11.0% (3.74%), the flow rate increases by 2.9% (20.17 cc/rev), and the specific slipping and pressure angle greatly decrease by 41.6% (1.35) and 33.1% (18.38°), respectively.

$$q_i(\alpha) = \frac{1}{2} b \left[\left(\left|\overrightarrow{O_1M}\right|^2 - \left|\overrightarrow{O_1N}\right|^2 \right) \frac{r_2}{r_1} - \left(\left|\overrightarrow{O_2M}\right|^2 - \left|\overrightarrow{O_2N}\right|^2 \right) \right] \omega_1$$

$$Q = z_1 \int_0^{2\pi} q(\alpha) d\alpha = z_1 \sum_{i=1}^{z_2} q_i \quad (6)$$

$$i = \frac{q_{max} - q_{min}}{q_{average}} \quad (7)$$

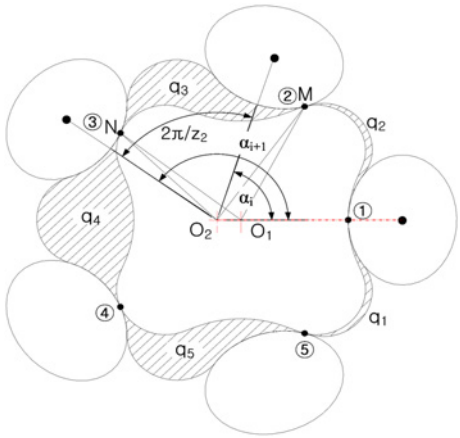

Fig. 6 Schematic model for calculating flow rate and irregularity

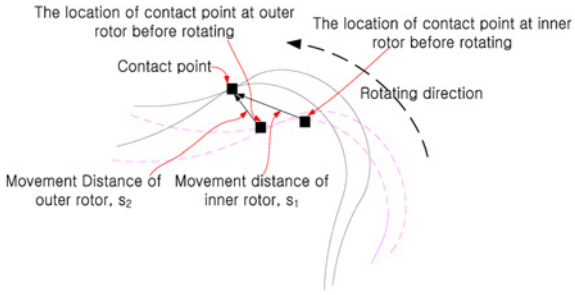

Fig. 7 Schematic model for calculating specific sliding

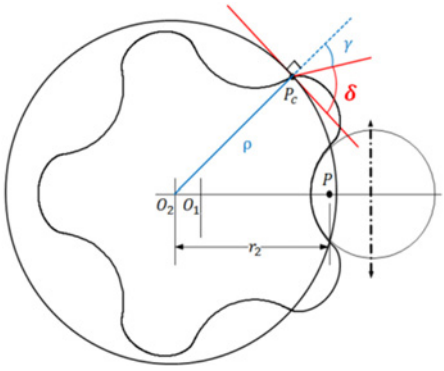

Fig. 8 Schematic model for calculating pressure angle

$$\text{specific sliding} = \frac{|s_2 - s_1|}{s_2} \quad (8)$$

$$\cos\gamma = \frac{\rho^2 + \overline{P_cP^2} - r_2}{2 \times \overline{P_cP^2} \times \rho} \quad (9)$$

$$\gamma = \cos^{-1}\left(\frac{\rho^2 + \overline{P_cP^2} - r_2}{2 \times \overline{P_cP^2} \times \rho} \right) \quad (10)$$

$$\delta = 90° - \gamma \quad (11)$$

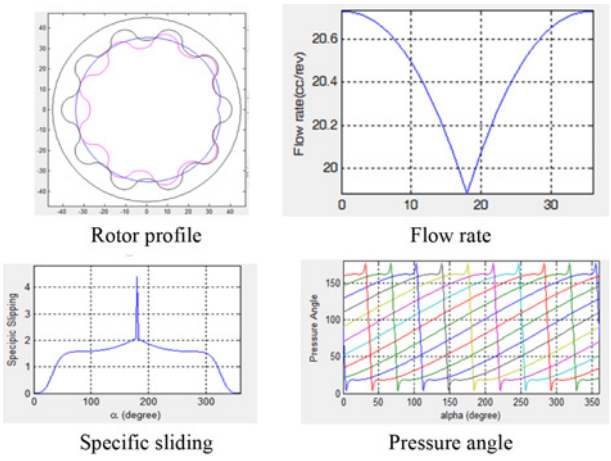

Fig. 9 Improved rotor profile and performance values

Table 1 Comparison of performance parameters of existing and 2-ellipses

	Flow rate (cc/rev)	Irregularity (%)	Specific slipping	Pressure angle (°)
Existing (circle)	19.61	3.37	2.31	27.47
2-ellipses	20.17 (2.9%↑)	3.74 (11.0%↑)	1.35 (41.6%↓)	18.38 (33.1%↓)

Table 2 Results of noise tests of the developed gerotor (2-ellipses) and the existing one (3-ellipses)

Type of lobe shape	Noise (dB)
3-ellipses	77.7 (2500 rpm)
2-ellipses	75.7 (2500 rpm)

Based on the results of the performance parameters in case of 2-ellipses, it is observed that specific sliding is 6.82% higher, which brings a negative effect on noise, than those in case of 3-ellipses, while 0.26% lower irregularity and 5.57% lower pressure angle in case of 2-ellipses bring a positive effect on noise. Therefore, the actual noise tests regarding to the lobe shapes generated in both cases at 2500 rpm indicate that the developed gerotor (2-ellipses) has 2.6% lower noise than the existing one (3-ellipses) as shown in Table 2, and that drastic change of curvature has totally a negative effect on noise.

Also, comparing the inner lobe shape of geortor (2-ellipses) generated to the existing 3-combined lobe shape (3-ellipses), the latter has steeper change of curvature than the former, as shown in Fig. 10.

Also, Table 3 shows order of priority regarding to the design parameters affecting the performances.

4. Port Design using CFD Analysis

4.1 Governing equations for CFD analysis

In order to perform a CFD analysis of the oil pump, we assumed that the fluid is Newtonian and incompressible, initially stationary (initial velocity = 0), isothermal, and turbulent. The fundamental equations to be numerically solved by the CFD code are the conservation of mass,

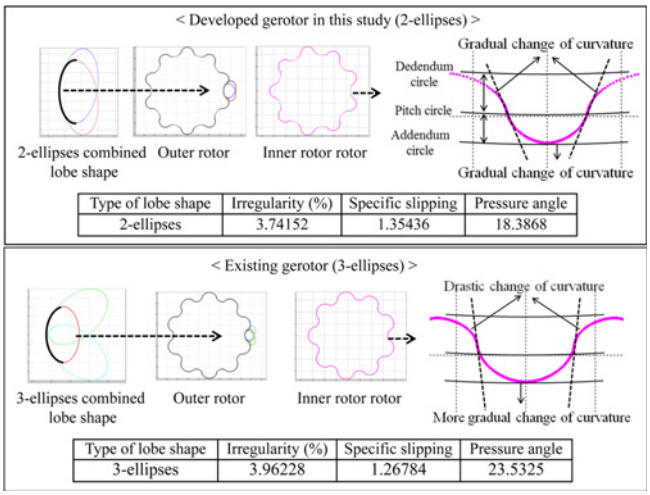

Fig. 10 Comparison of lobe profiles and performance parameters of developed gerotor (2-ellipses) with those of the existing 3-combined gerotors (3-ellipses)

Table 3 Order of priority regarding to the design parameters affecting the performance parameters

Order of priority	Flow rate	Irregularity	Specific slipping	Pressure
1	d	d	d	d
2	rl_2	rl_2	rl_2	η
3	η	k_1	γ	γ
4	k_1	η	k_1	rl_2
5	γ	γ	η	k_1

momentum, and energy, and these equations can be written, respectively, in basic integral representation as Eqs. (12)~(14).[7] $\Omega(t)$ and σ are a control volume and its surface, respectively; n is a surface vector pointed outward; ρ, p, and v are the density, pressure, and velocity of the fluid, respectively; f is a body force; and v_δ is a surface motion velocity. The shear stress tensor $\tilde{\tau}$ is a function of fluid viscosity (μ) as shown in Eq. (15),[8] where u_i (i = 1, 2, 3) is a velocity component and δ_{ij} is the Kronecker delta function.[7] Turbulence models for computing effective liquid viscosities are important at high Reynolds numbers, especially in rotor dynamic types of pumps where viscous forces and turbulent mixing can strongly affect the flow rate and pressure. Turbulence can be considered by applying the standard k-epsilon model (Eqs. (16) and (17)), and an eddy viscosity turbulent model that is derived from a Reynolds-averaged Navier-Stokes (RANS) equation by using the ANSYS CFD code. In Eqs. (16) and (17), G_t is a turbulent generation term; k is the turbulent kinetic energy; c_1 and c_2 are Prandtl numbers; and σ_k and σ_ε are the turbulent kinetic energy dissipation rates.[8]

$$\frac{\partial}{\partial t}\int_{\Omega(t)}\rho d\Omega+\int_{\sigma}\rho(\upsilon-\upsilon_\sigma)nd\sigma=0 \tag{12}$$

$$\frac{\partial}{\partial t}\int_{\Omega(t)}\rho d\Omega+\int_{\sigma}\rho((\upsilon-\upsilon_\sigma)n)vd\sigma=\int_{\sigma}\tilde{\tau}nd\sigma-\int_{\sigma}pnd\sigma+\int_{\Omega}fd\Omega \tag{13}$$

$$\frac{\partial}{\partial t}\left[\rho\left(u+\frac{\upsilon^2}{2}+gz\right)\right]+\nabla\left[\rho\upsilon\left(h+\frac{\upsilon^2}{2}+gz\right)\right]+\nabla Q-\nabla(T_d\upsilon)=0 \tag{14}$$

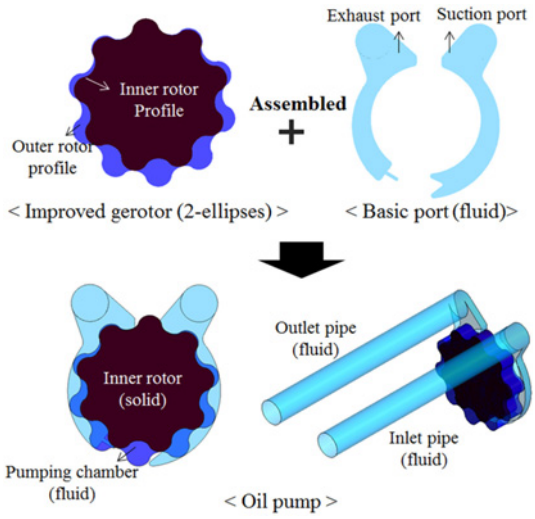

Fig. 11 Oil pump assembled with the improved gerotor (2-ellipses-combined lobe shape) and port

$$\tau_{ij} = \mu\left(\frac{\partial u_i}{\partial x_j} + \frac{\partial u_j}{\partial x_i}\right) - \frac{2}{3}\mu\frac{\partial u_k}{\partial x_k}\delta_{ij} \tag{15}$$

$$\frac{\partial}{\partial t}\int_{\Omega(t)} \rho k \, d\Omega + \int_{\sigma} \rho((\upsilon - \upsilon_\sigma)n)d\sigma = \left(\int_{\sigma}\left(\mu + \frac{\mu_t}{\sigma_k}\right)(\nabla k n)d\sigma + \int_{\Omega}(G_t - \rho\varepsilon)d\Omega\right) \tag{16}$$

$$\frac{\partial}{\partial t}\int_{\Omega(t)} \rho\varepsilon \, d\Omega + \int_{\sigma} \rho((\upsilon - \upsilon_\sigma)n)\varepsilon d\sigma = \int_{\sigma}\left(\mu + \frac{\mu_t}{\sigma_\varepsilon}\right)(\nabla\varepsilon n)d\sigma + \int_{\Omega}\left(c_1 G_t\frac{\varepsilon}{k} - c_2\rho\frac{\varepsilon^2}{k}\right)d\Omega \tag{17}$$

4.2 CFD analysis models

A gerotor oil pump is comprised of an inner rotor, the pumping chamber (which is between the inner rotor and the outer rotor), the inlet and outlet pipes, and the suction and exhaust ports, as shown in Fig. 11. When the volume of the pumping chamber on the suction side increases as the gerotor rotates, the working oil is taken in from the inlet pipe. When the volume of the pumping chamber on the exhaust side decreases, the working oil is exhausted through the outlet pipe.

In order to improve fuel efficiency, a CFD model of the oil pump was constructed. The port shape was assembled with the improved gerotor with 2-ellipses-combined lobe shape in chapter 2. On the basis of experience accumulated in the field, four geometric parameters relating to the port shape were chosen for improving the performance of the oil pump. First, in order to decrease the sudden pressure variation when the working oil flows from the pumping chamber into the exhaust port, a 20° inclined port was considered (Model 1, Fig. 12(b)). To improve the volume efficiency of the oil pump, the fluid volume of the entrance was expanded by changing the inlet pipe into two inlet pipes which have 20 mm diameter (Model 2, Fig. 12(c)). The upper part of the suction port is convex (Model 3, Fig. 12(d)), using a part of the ellipse (major axis 18 mm, minor axis 8 mm). Also, the 30 mm rounded

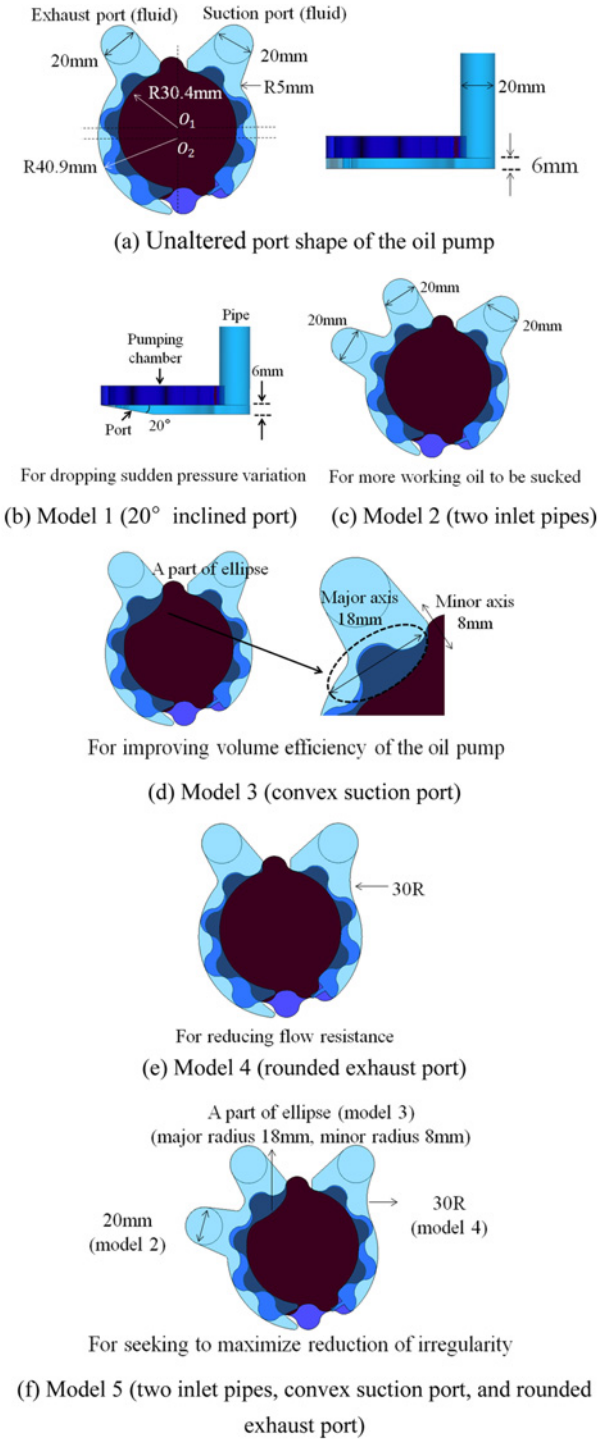

Fig. 12 3-D models for CFD analyses

upper part of the exhaust port (Model 4, Fig. 12(e)) was modeled to mitigate flow resistance and to make the streamline stable.

We assembled the improved gerotor (2-ellipses-combined lobe shape) with the modified port shapes, and fluid analyses of the four models were performed with ANSYS CFD commercial software. By comparing the results with the results from the existing oil pump, assembled with the improved gerotor (2-ellipses combined lobe shape) and altered port shape, the effects of the aforementioned geometric parameters on flow rate and irregularity were investigated.

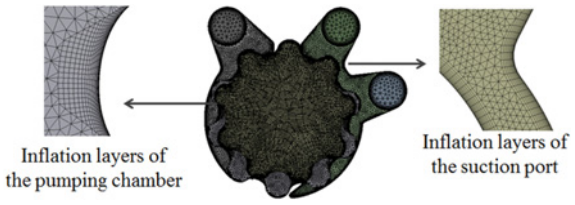

Fig. 13 Mesh for CFD analysis

Fig. 14 k-epsilon turbulent model and convergence criteria

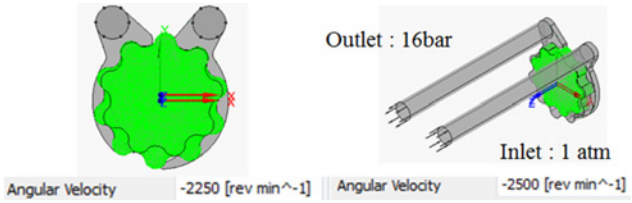

Fig. 15 Rotational velocities and boundary conditions

Table 4 Material properties of ATF

Temperature	Density	Kinematic viscosity	Dynamic viscosity
80°C	799.7 kg/m^3	8.2 mm^2/s	0.0066 kg/ms

4.3 CFD analysis conditions

The inflation mesh for generating thin cells adjacent to the surface of the fluid field were created with 20 layers and a 3 mm inflation thickness to take into account the viscous boundary layer. The mesh size of the pumping chamber and port is 0.9 mm and that of the inlet/outlet pipes is 2 mm, applying a tetragonal grid as shown Fig. 13. Since the shape of the pumping chamber changes according to time as the gerotor rotates, the transient flow equations were used, and turbulent flow was taken into account by the standard k-e model. The inner rotor rotates 360° in a clockwise direction for 0.024 s at 2500 rpm. Iterations were run for every time step (6.0×10^{-6} s) to reach convergence criterion, which was set as a residual value of 10^{-4} for flow stabilization, as shown Fig. 14. According to the ratio of the number of teeth of the inner rotor and outer rotor (9/10), the rotational velocity of the pumping chamber is 2,250 rpm as shown Fig. 15. After the working oil is sucked from the inlet pipe at 1atm, it is exhausted through the outlet pipe at 16 bar. The material properties of the automatic transmission fluid used in vehicles at 80°C are shown in Table 4.

4.4 Results of CFD analysis

After deriving the flow rates of the considered models at the outlet pipes according to rotation times, the average flow rates and their

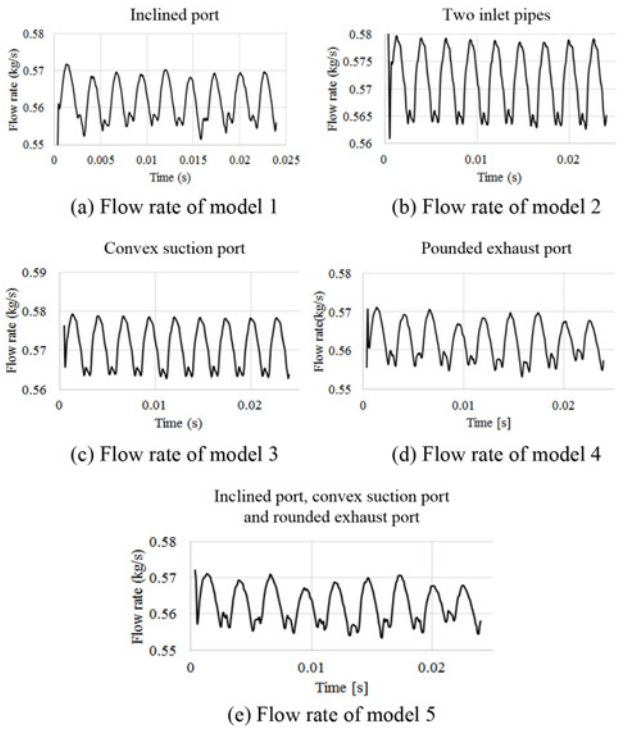

Fig. 16 Flow rates versus time

Table 5 Results of flow rates and irregularity, comparing all models with the existing oil pump

	Flow rate (kg/s)	Irregularity (%)
	Error (%)	Error (%)
Existing	0.5613	2.7871
Model 1 (Inclined port)	0.5618 (0.09%↑)	2.7722 (0.54%↓)
Model 2 (2 inlet pipes)	0.5713 (1.78%↑)	2.7026 (3.03%↓)
Model 3 (Convex suction port)	0.5709 (1.71%↑)	2.6628 (4.46%↓)
Model 4 (Rounded exhaust port)	0.5623 (0.17%↑)	2.4883 (12.01%↓)
Model 5	0.5625 (0.21%↑)	2.3744 (14.81%↓)

irregularities were calculated during one revolution of the gerotor, except for the initially unstable flow rates obtained from 0 to 0.003 s, as shown in Fig. 16 and Table 5. In the case of model 1, the flow rate (0.09%↑) and irregularity (0.54%↓) were slightly better than the existing oil pump, assembled with the improved gerotor (2-ellipses combined lobe shape) and unaltered port shape, whereas the flow rates in the case of model 2 and model 3 were 1.78% (0.5713 kg/s) and 1.71% (0.5709 kg/s) higher than the existing oil pump's flow rate, respectively. The irregularities of those decreased by 3.03% (2.7026%) and 4.46% (2.6628%). Especially, model 4 shows a much lower irregularity of 2.4883% (12.01%↓) and a higher flow rate of 0.5623 kg/s (0.17%↑) than in the case of the existing oil pump.

Based on the CFD results, in order to improve the flow rate of the oil pump, the volume of the inlet pipe or the suction port must be expanded. However, it is difficult to increase the flow rate greatly, because the flow rate is mainly affected by the volume of the pumping chamber. On the other hand, by changing the port shape, a stable and

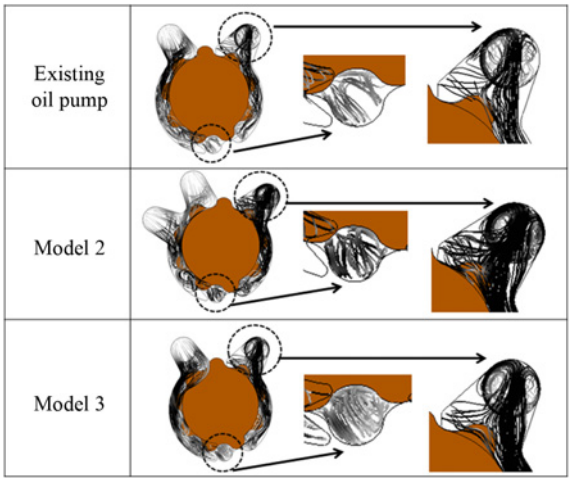

Fig. 17 Comparing streamlines of the existing oil pump with those of models 2 and 3

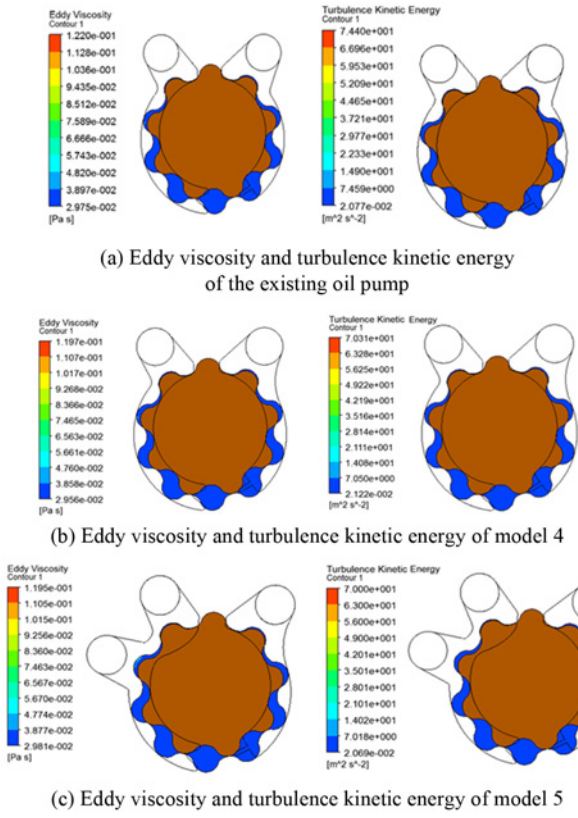

Fig. 18 Eddy viscosities and turbulence kinetic energies of the existing model, model 4, and model 5

smooth streamline enables irregularity to be significantly reduced. Therefore, to maximize the reduction of noise, a CFD analysis of model 5 (Fig. 12(e)) was performed. The analysis considered three suggested models (two inlet pipes, a convex suction port, and a rounded exhaust port). Although the irregularity of model 5 is not equal to the summation of the amounts of irregularities to be decreased (model 2 + model 3 + model 4) due to the interaction of flow, it has the lowest irregularity

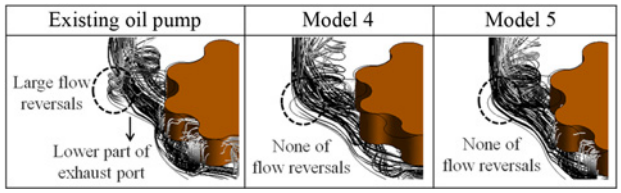

Fig. 19 Comparison of flow reversal of the existing model, model 4 and model 5 oil pumps

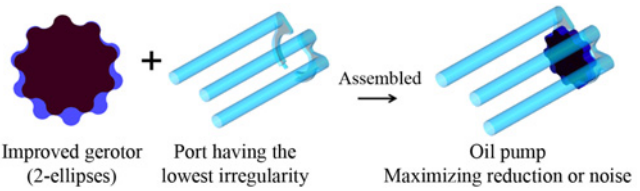

Fig. 20 Oil pump (the improved gerotor + the proposed port) to maximize noise reduction

(14.81% lower) among five models suggested in this study.

In the cases of model 2 and model 3, the streamlines at the highlighted parts in Fig. 17 are denser than those of the existing oil pump. Thus, flow rates of the suggested models were increased because of higher volume efficiency than that of the existing model. Compared to the CFD results of the existing oil pump, the eddy viscosities of model 4 and model 5 decreased by 1.88% and 2.05%, respectively, and their turbulence kinetic energies were 5.50% and 5.91% lower, respectively, as shown in Fig. 18. Also, as the results of analyzing the streamlines, the flow reversals of model 4 and model 5 at the lower part of the exhaust port disappeared, as shown in Fig. 19. Thus, the irregularities are greatly reduced.

4.5 The combined effect of lobe shape and port design

Based on the theoretical calculation to consider only rotor profiles rather than port shapes, an increased flow rate leads to increased irregularity. But, when considering both the port shapes and rotor profile, an increased flow rate and decreased irregularity were observed.

Although the irregularity of the improved gerotor with a 2-ellipses-combined lobe shape was 11.0% higher than that of the existing model, the proposed oil pump (model 5) has a 14.8% lower irregularity through re-designing the port shape. In conclusion, by assembling the improved gerotor with the proposed port (model 5), the irregularity, specific sliding, and pressure angle are reduced by 3.8%, 41.6%, and 33.1%, respectively. Thus, noise reduction seems to be maximized as show in Fig. 20.

5. Conclusion

We propose port shapes for improving the performance of an oil pump (flow rate and irregularity) having the improved gerotor with a 2-ellipses-combined lobe shape, based on CFD analysis. Our conclusions can be summarized as follows:

1. For improving fuel efficiency and reducing the noise of the oil pump, new port shapes (two inlet pipes, a convex suction port, an inclined exhaust groove, and a convex exhaust port) are proposed through performing CFD analyses.

In the new design, the volume efficiencies are increased and flow rates are higher than the existing oil pump, as a result of expanding the fluid volume of the entrance (two inlet pipes and a convex suction port).

Flow resistances of the oil pumps (two inlet pipes, a convex suction port, and a rounded exhaust port) were mitigated, and lower eddy viscosity and turbulence kinetic energy lead irregularities to be reduced.

Model 5 exhibits the lowest irregularity (14.81%↓) as a result of combining three geometric parameters at the same time.

2. The performance improvement of the oil pump was maximized, by re-designing port shape assembled with the improved gerotor (2-elipses combined lobe shape).

3. Automated design and multiple calculation programs were developed for generating a 2-ellipses-combined lobe shape. We derived the improved design by predicting performances on the basis of theoretical analysis.

The proposed port shape can be adopted in various fields. In further research, the improved design of a port shape will be carried out in order to maximize the improvement of fuel efficiency and the reduction of noise.

ACKNOWLEDGEMENT

This research was supported by the Basic Science Research Program through the National Research Foundation of Korea (NRF), funded by the Ministry of Education of the Korean government (no. 2014R1A1A 4A01009110). The authors gratefully acknowledge this support.

REFERENCES

1. Jung, S.-Y., Bae, J.-H., Kim, M.-S., and Kim, C., "Development of a New Gerotor for Oil Pumps with Multiple Profiles," Int. J. Precis. Eng. Manuf., Vol. 12, No. 5, pp. 835-841, 2011.

2. Mimmi, G. C. and Pennacchi, P. E., "Non-Undercutting Conditions in Internal Gears," Mechanism and Machine Theory, Vol. 35, No. 4, pp. 477-490, 2000.

3. Demenego, A., Vecchiato, D., Litvin, F. L., Nervegna, N., and Mancó, S., "Design and Simulation of Meshing of a Cycloidal Pump," Mechanism and Machine Theory, Vol. 37, No. 3, pp. 311-332, 2002.

4. Kim, J.-H., Kim, C., and Chang, Y. J., "Optimum Design on Lobe Shapes of Gerotor Oil Pump," Journal of Mechanical Science and Technology, Vol. 20, No. 9, pp. 1390-1398, 2006.

5. Bae, J. H., Lee, H. R., and Kim, C., "Optimal Design of Gerotor with Combined Profiles (Three-Ellipse and Ellipse-Involute-Ellipse) Using Rotation and Translation Algorithm," Transactions of the Korean Society of Mechanical Engineers A, Vol. 39, No. 2, pp. 169-177, 2015.

6. Bae, J. H., Kwak, H. S., San, S., and Kim, C., "Design and CFD Analysis of Gerotor with Multiple Profiles (Ellipse-Involute-Ellipse Type and 3-Ellipses Type) Using Rotation and Translation Algorithm," Proceedings of the Institution of Mechanical Engineers, Part C: Journal of Mechanical Engineering Science, DOI No. 10.1177/0954406215583888, 2015.

7. Ding, H., Visser, F. C., Jiang, Y., and Furmanczyk, M., "Demonstration and Validation of a 3D CFD Simulation Tool Predicting Pump Performance and Cavitation for Industrial Applications," Journal of Fluids Engineering, Vol. 133, No. 1, Paper No. 011101, 2011.

8. Frosina, E., Senatore, A., Buono, D., Manganelli, M. U., and Olivetti, M., "A Tridimensional CFD Analysis of the Oil Pump of an High Performance Motorbike Engine," Energy Procedia, Vol. 45, pp. 938-948, 2014.

9. Kumar, M. S. and Manonmani, K., "Computational Fluid Dynamics Integrated Development of Gerotor Pump Inlet Components for Engine Lubrication," Proceedings of the Institution of Mechanical Engineers, Part D: Journal of Automobile Engineering, Vol. 224, No. 12, pp. 1555-1567, 2010.

10. Hsieh, C.-F., "Flow Characteristics of Gerotor Pumps with Novel Variable Clearance Designs," Journal of Fluids Engineering, Vol. 137, No. 4, Paper No. 041107, 2015.

11. Kim, S.-Y., Nam, Y.-J., and Park, M.-K., "Design of Port Plate in Gerotor Pump for Reduction of Pressure Pulsation," Journal of Mechanical Science and Technology, Vol. 20, No. 10, pp. 1626-1637, 2006.

12. Nam, K.-W., Jo, S.-H., and Park, J.-I., "Numerical Simulation in the IC Engine Lubricating Gerotor Oil Pump," Transactions of the Korean Society of Mechanical Engineers B, Vol. 30, No. 10, pp. 1019-1025, 2006.

13. Kwak, H. S., Li, S. H., and Kim, C., "Performance Improvement of Oil Pump by Design of Gerotor (Combined Profile-Two Ellipses) and Port," J. Korean Soc. Precis. Eng., Vol. 33, No. 3, pp. 207-216, 2016.